Rongqing Chen*, Alberto Battistel, Sabine Krueger-Ziolek, James Geoffrey Chase, Stefan J. Rupitsch, and Knut Moeller

Assessing the impact of a structural prior mask on EIT images with different thorax excursion models

https://doi.org/10.1515/cdbme-2023-1092

Abstract: Electrical Impedance Tomography (EIT) has shown promising results as a low-cost imaging method for visualizing ventilation distribution within the lungs. However, clinical interpretation of EIT images is often hindered by blurred anatomical alignment and reconstruction artifacts. Integrating structural priors into the EIT reconstruction process has the potential to enhance the interpretability of the EIT images. Thus, a patient-specific structural prior mask is introduced in this contribution, which restricts the reconstruction of conductivity changes within the lung regions. We conducted numerical simulations on four finite element models representing four different thorax excursions to investigate the impact of the structural prior mask on EIT images. Simulations were performed under four different ventilation statuses. EIT images were reconstructed using the Gauss-Newton and discrete cosine transform-based EIT algorithms. We conducted a quantitative analysis using figures of merit to evaluate the images of the two reconstruction algorithms. The results show the structural prior mask preserves the morphological structures of the lungs and limits reconstruction artifacts.

Keywords: Electrical impedance tomography, structural prior, thorax shape, algorithm

1 Introduction

Electrical Impedance Tomography (EIT) is a medical imaging technique commonly used at the bedside to visualize the ventilation distribution within the lungs. Its value lies in providing real-time insight into ventilation distribution, which can aid in the adjustment of ventilator settings, particularly for patients with Acute Respiratory Distress Syndrome (ARDS) in Intensive Care Units (ICU) [1]. EIT's benefits include reducing Ventilator Induced Lung Injury (VILI) in mechanical ventilation. Despite its advantages, the reconstruction of EIT images remains an ill-posed inverse problem with significant degrees of freedom.

Various algorithms have been proposed to decrease these degrees of freedom, such as the spectral graph wavelets regularized algorithm [2] and Discrete Cosine Transformation (DCT) based EIT algorithm [3]. However, EIT images are still characterized by low spatial resolution, blurred anatomical alignment, and reconstruction-induced artifacts, hindering interpretation in clinical settings. A patient-specific structural prior mask, derived from other morphological imaging modalities such as CT, has the potential to offer more comprehensive insights on the anatomical structure of the lungs, thus, confining EIT reconstruction to lung regions [3].

This work investigates the influence of a personalized structural prior mask on EIT reconstructions using different thorax excursion models. Four 3D models with different thorax excursions were subjected to numerical simulations under four different ventilation statuses. EIT images were reconstructed using the Gauss-Newton (GN) algorithm and DCT-based EIT algorithm, and the influence of the structural prior mask was evaluated quantitatively using figures of merit. We conducted further statistical analysis to determine if there is a significant difference between the EIT results reconstructed with and without the structural mask.

2 Methods

2.1 Reconstruction of EIT images

EIT aims to reconstruct the variation of electrical conductivity distribution $\mathbf{x} = \boldsymbol{\sigma}_2 - \boldsymbol{\sigma}_1$ within the thorax from the boundary voltage measurements $\mathbf{y} = \mathbf{v}_2 - \mathbf{v}_1$. However, this problem is ill-posed because the accurate conductivity distribution varia-

***Corresponding author: Rongqing Chen,** Institute of Technical Medicine, Furtwangen University, Jakob-Kienzle-Str. 17, Villingen-Schwenningen, Germany; Faculty of Engineering, University of Freiburg, Georges-Köhler-Allee 101, Freiburg, Germany, e-mail: rongqing.chen@hs-furtwangen.de
Alberto Battistel, Sabine Krueger-Ziolek, Knut Moeller, Institute of Technical Medicine, Furtwangen University, Jakob-Kienzle-Str. 17, Villingen-Schwenningen, Germany
James Geoffrey Chase, Department of Mechanical Engineering, University of Canterbury, Private Bag 4800, Christchurch 8140, New Zealand
Stefan J. Rupitsch, Faculty of Engineering, University of Freiburg, Georges-Köhler-Allee 101, Freiburg, Germany

Open Access. © 2023 The Author(s), published by De Gruyter. This work is licensed under the Creative Commons Attribution 4.0 International License.

tion is not linearly related to the boundary measurements of the voltage changes.

The widely applied time-difference EIT reconstruction algorithm with regularization assumes the conductivity changes $\mathbf{x}$ are small. As the conductivity properties of the thorax tissue are inhomogeneous, a finite element model (FEM) is required to discretize the domain spatially. The estimation of the changes in conductivity $\hat{\mathbf{x}}$ from a set of changes in boundary voltages $\mathbf{y}$ is formed through a minimization approach

$$\hat{\mathbf{x}} = (\mathbf{J}^\intercal\mathbf{J} + \lambda^2\mathbf{R})^{-1}\mathbf{J}^\intercal\mathbf{y} = \mathbf{B}\mathbf{y}\,, \tag{1}$$

where $\mathbf{J}$ is the Jacobian matrix, which maps the voltage variations to the conductivity change and is derived from the reference $\boldsymbol{\sigma}^{ref}$ as $J_{i,j} = \frac{\partial y_i}{\partial x_j}\Big|\boldsymbol{\sigma}^{ref}$, where the element $J_{i,j}$ maps small voltage changes at the position i of $\mathbf{y}$ to a conductivity change of the element j within the FEM. $\boldsymbol{\sigma}^{ref}$ is a pre-selected conductivity distribution reference. $\mathbf{y}$ is usually normalized in time-difference EIT. $\mathbf{R}$ is a regularization to linearize the inverse problem, λ is the hyperparameter to control the regularization. $\mathbf{B}$ is the reconstruction matrix.

The degrees of freedom of the inverse problem could be reduced by clustering the elements of the FEM. In this paper, we use a subset $\mathbf{D}$ of basic cosine functions from the DCT at varying frequencies

$$D(p,q) = \alpha_p\alpha_q \cos\frac{(2m+1)p\pi}{2M}\cos\frac{(2n+1)q\pi}{2N}\,, \tag{2}$$

where p and q are the frequencies of the cosine functions at x-axis and y-axis, respectively. Here, p and q were chosen as 15 frequencies for both axes. The desired EIT image size is $M \times N$, and (m,n) is the position of a pixel.

To improve interpretability, a structural prior mask $\mathbf{P}$ derived from a morphological image, e.g., CT, can be integrated into the EIT reconstruction process:

$$C(p,q)_{m,n} = P_{m,n} \cdot D(p,q)_{m,n}\,, \tag{3}$$

where the matrix $\mathbf{P}$ specifies the shape of the lungs. Using the matrix $\mathbf{D}(p,q)$ (without prior) or $\mathbf{C}(p,q)$ (with prior), the columns of the basic function subset are calculated as $\mathbf{K}^{np}_j = T(\mathbf{D}(p,q))$ or $\mathbf{K}^{p}_j = T(\mathbf{C}(p,q))$. T is a map that assigns every pixel in $\mathbf{D}(p,q)$ or $\mathbf{C}(p,q)$ to the element in the FEM that covers the pixel. j is the column index.

The Jacobian matrix $\mathbf{J}$ is modified by the subset matrix $\mathbf{K}$ as $\mathbf{J}_{DCT} = \mathbf{J}\cdot\mathbf{K}$. $\mathbf{J}_{DCT}$ maps the voltage variations to the changes in DCT coefficients. Then, the solution to the inverse problem is represented by the changes of DCT coefficients $\hat{\mathbf{x}}_{DCT}$, similar to Equation (1). The $\hat{\mathbf{x}}_{DCT}$ are used to restore the EIT image $\mathbf{H}$ through the inverse DCT calculation

$$\mathbf{H} = \sum_{p=0}^{n_{xDCT}}\sum_{q=0}^{n_{yDCT}} \mathbf{C}(p,q)\cdot\hat{x}_{DCT,j} \tag{4}$$

This paper uses Tikhonov regularization $\mathbf{R} = \mathbf{I}$ for all the algorithms. The optimal hyperparameter λ is selected based on when the noise figure (NF) reaches 0.5.

2.2 Simulation data

We evaluated the effect of the structural prior mask on EIT reconstructions with numerical simulations using the EIDORS toolbox [4] in MATLAB R2019a (Mathworks, Natick, MA, USA). Netgen generated four different FEM models, each with a distinct thorax excursion [5]. Figure 1 shows the thorax excursions and their respective FEMs (2D projection of the respective 3D model). As an illustration, the 3D FEM of Model 4 is presented in Figure 2. In the initial configuration, FEM elements unrelated to lung region were assigned a conductivity of $\boldsymbol{\sigma}^{initial}_{non-lung} = 1$, while those related to lung tissue were set to $\boldsymbol{\sigma}^{initial}_{lung} = 0.5$. The voltage measurement $\mathbf{v}^{initial}$ was generated and used as the reference for the reconstruction. We conducted simulations of four different ventilation patterns:

a. Right dorsal lung has no ventilation;
b. Most ventral and dorsal parts of both lungs have no ventilation;
c. Ventral left and right dorsal lungs have no ventilation;
d. Dorsal parts of both lungs have no ventilation.

The boundary voltage measurement $\mathbf{v}^{vent}_i$ was generated for each simulation setting by assigning $\boldsymbol{\sigma}^{vent}_{lung} = 0.25$ to the ventilated lung areas. To account for measurement noise, 1% Gaussian noise was added to the boundary measurement $\mathbf{v}^{vent}_i$ before reconstruction. To prevent the 'inverse crime', we used a coarser FEM mesh with the same thorax excursion for the reconstruction. The lung shape shown in Figure 1 was introduced into the reconstruction as the structural prior mask.

2.3 Evaluation of the EIT images

We introduced figures of merit to quantitatively analyze the EIT images, which can only be applied to simulations since the ground truth is known. The evaluation begins by defining a lung region $\mathbf{H}^{lung}$ using a threshold of 20% of the maximum pixel value in an EIT reconstruction $\mathbf{H}$.

The *position error* evaluates the accuracy of the reconstructed position of the lungs. It is the shift of the center of gravity (G) of both the left and right lungs in $\mathbf{H}$ from the $\mathbf{H}^{GT}$

$$\text{PE} = \|G^{GT}_l - G^{H}_l\| + \|G^{GT}_r - G^{H}_r\|\,. \tag{5}$$

The *shape deformation* quantitatively evaluates the deviation of the corresponding lung regions in an EIT image $\mathbf{H}^{lung}$

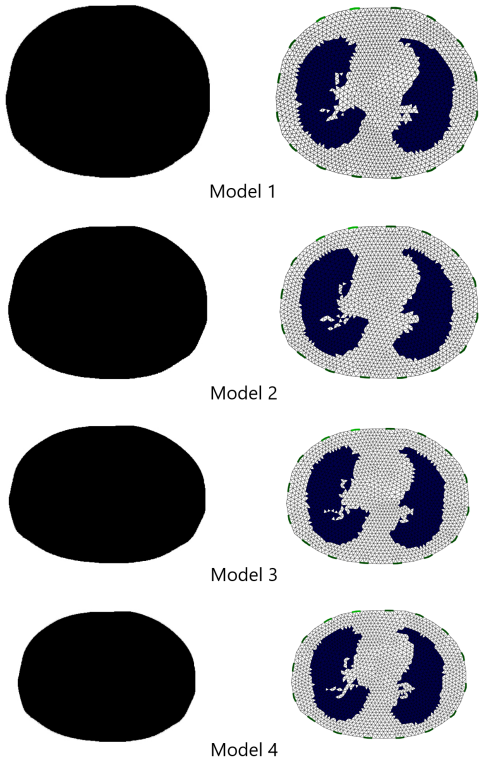

Fig. 1: Thorax excursions and corresponding FEMs (2D projection from the 3D model) used for simulations.

from the lung region $\mathbf{P}$ in ground truth $\mathbf{H}^{GT}$

$$\mathrm{SD} = \|\mathbf{H}_l^{lung} - \mathbf{P}\|_1 / \|\mathbf{P}\|_1 \,. \tag{6}$$

The *ring effect* is defined as the ratio of the sum of the negative pixel values to the sum of the absolute pixel values in an EIT reconstruction $\mathbf{H}$

$$\mathrm{R} = \sum_{i,j} |H_{i,j}^{<0}| / \sum_{i,j} |H_{i,j}| \,, \tag{7}$$

where the $H_{i,j}^{<0}$ is the set of pixels in the EIT image $\mathbf{H}$ with values less than 0.

The *amplitude response* is calculated as the ratio of the sum of the pixel values in the EIT reconstruction $\mathbf{H}$ to the sum of the pixel values in the corresponding ground truth $\mathbf{H}^{GT}$

$$\mathrm{AR} = \sum_{i,j} H_{i,j} / \sum_{i,j} H_{i,j}^{GT} \,. \tag{8}$$

amplitude response should be stable.

The *resolution* quantifies the size of reconstructed lungs relative to the entire reconstructed image

$$\mathrm{RES} = \sqrt{A^{lung}/A} \,, \tag{9}$$

where A^{lung} represents the pixel numbers in the reconstructed lung area, and A is the total pixel numbers of the EIT image $\mathbf{H}$. Please note that *resolution* should be small and stable.

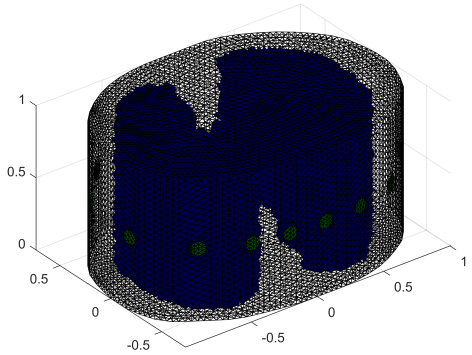

Fig. 2: The 3D FEM representing Model 4.

3 Results and Discussion

The conductivity reconstructions from the four ventilation patterns on Model 4 are presented as an example in Figure 3, where all pixels were normalized between -0.5 to 0.5 for comparison purposes. The black areas indicate no conductivity change, while blue or purple areas represent conductivity decrease or increase, respectively. In the first row of Figure 3, the simulated conductivity changes, i.e., the ground truth, were depicted. The second and third rows illustrate the GN approach reconstructions without or with a structural prior mask, respectively. The fourth and fifth rows show the DCT approach reconstructions without or with a structural prior mask, respectively. The EIT reconstructions without a structural prior mask lead to blurred edges and strong ring effects in both the GN and DCT methods.

Figure 4 presents the figures of merit of the reconstructions of four simulation patterns. Consistent with the qualitative results in Figure 3, the reconstructions from the GN method without a structural prior mask show the highest position error, shape deformation, ring effects, and resolution. Incorporating a structural prior mask improves the position error, shape deformation, ring effects, and resolution in both GN and DCT methods. Moreover, the amplitude response is more stable after introducing the structural mask.

The independent *t*-test was performed on the figures of merit to determine if there was a significant difference between the results obtained with and without the structural mask. The *t*-test was conducted only within the same algorithm. The figures of merit showed a statistically significant difference ($p < 0.001$) were marked with an asterisk ($\star$) in Figure 4. There was no significant difference found for the *position error* with or without a mask in both GN ($p = 0.24$) and DCT ($p = 0.18$) approaches. Similarly, no significant difference was found for the *ring effect* in the GN approach ($p = 0.02$).

It is worth noting that the structural prior masks used in this study were derived from the ideal simulations. However,

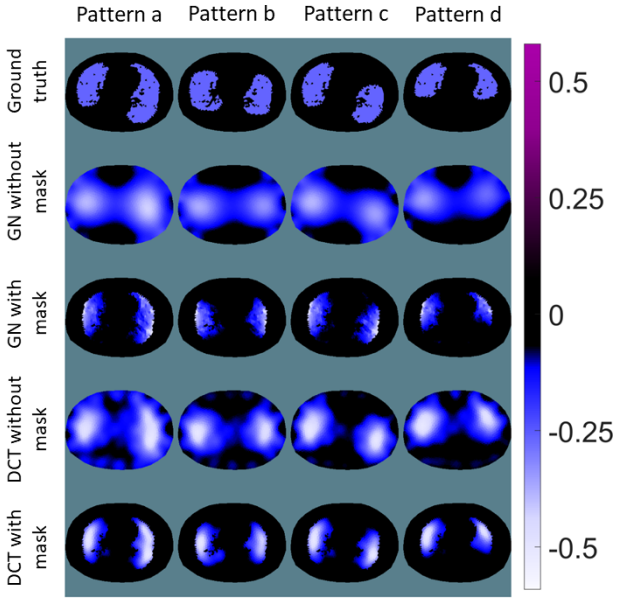

Fig. 3: Ground truth of the simulation on Model 4 and EIT reconstructions using GN and DCT approaches with and without a structural prior mask.

in clinical settings, these masks are usually derived from a single time-point CT or MRI, while EIT aims to show the continuously changing patient status. As a result, ensuring the accuracy of the structural prior masks become crucial when incorporating it into EIT reconstruction. Regular checks of the implemented structural prior masks are necessary to maintain its precision. It is important to note that the introduced structural mask does not seem to significantly improve the position accuracy in EIT images, and further investigation is necessary.

A limitation of this study is it solely relied on simulation experiments to assess the impact of the structural prior mask. To validate the effectiveness of the approach in real-world scenarios, it is imperative to conduct further studies using phantom experiments and clinical data. Additionally, in clinical settings, the use of the center of ventilation may be more appropriate than the center of gravity currently used in this study when calculating position error. However, our evaluation simulated a homogeneous conductivity distribution within the ventilated lung region, resulting in the center of gravity and center of ventilation being the same.

Nevertheless, the results of this study demonstrate incorporating a structural prior mask improves the interpretability of EIT images, resulting in more accurate localization of conductivity changes within the lungs.

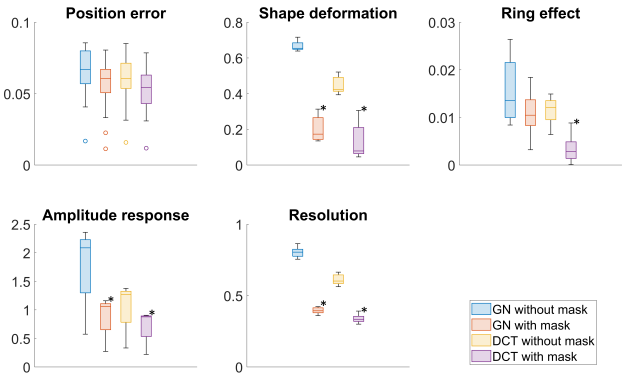

Fig. 4: Figures of merit for EIT reconstructions. Asterisk ($\star$) indicates significant difference between results with and without the structural mask compared within the same algorithm.

4 Conclusion

The implementation of an accurate structural prior mask can improve the interpretability of EIT images. This approach can provide valuable insights into the pathophysiology of the lungs in clinical settings, as it allows for a direct correlation between regional lung behavior and morphological structures.

Author Statement

Research funding: This research was partially supported by German Federal Ministry of Education and Research (MOVE 13FH628IX6) and H2020 MSCA Rise (#872488 DCPM). Conflict of interest: Authors state no conflict of interest.

References

[1] Inéz. Frerichs et al. Chest electrical impedance tomography examination, data analysis, terminology, clinical use and recommendations: Consensus statement of the TRanslational EIT developmeNt stuDy group. *Thorax*, 72(1):83–93, January 2017. ISSN 1468-3296. 10.1136/thoraxjnl-2016-208357.

[2] Bo Gong, Benjamin Schullcke, Sabine Krueger-Ziolek, Marko Vauhkonen, Gerhard Wolf, Ullrich Mueller-Lisse, and Knut Moeller. EIT imaging regularization based on spectral graph wavelets. *IEEE Trans Med Imaging*, 36(9):1832–1844, 2017.

[3] B. Schullcke, B. Gong, S. Krueger-Ziolek, M. Soleimani, U. Mueller-Lisse, and K. Moeller. Structural-functional lung imaging using a combined CT-EIT and a discrete cosine transformation reconstruction method. *Sci. Rep.*, 6:25951, 2016.

[4] Andy Adler and William R. B. Lionheart. Uses and abuses of EIDORS: An extensible software base for EIT. *Physiological Measurement*, 27(5):S25–S42, 2006. ISSN 0967-3334. 10.1088/0967-3334/27/5/S03.

[5] Joachim Schöberl. NETGEN An advancing front 2D/3D-mesh generator based on abstract rules. *Computing and Visualization in Science*, 1(1):41–52, July 1997. ISSN 1432-9360. 10.1007/s007910050004.